calculations with and without this factor are shown in Figs. 3(a) and 3(b).

It should be noted that the spin-dependent terms for $L=1$ are not characteristic of Bessel and Weber functions of order $M=1$, but rather are described by functions of opposite parity, i.e., $M=0$ and $M=2$. It is for this reason that phase differences occur in $L=1$ reactions and characterize J. However, for $L=2$, the two spin states $J=\frac{5}{2}$ and $J=\frac{3}{2}$ are primarily characterized by distributions given by Eq. (1) with $M=1$ and $M=3$, respectively. These odd-M distributions do not oscillate, and consequently the determination of J at large angles for L even does not appear feasible.

The semiclassical explanation for the change in M by ± 1 for spin-dependent terms is relatively simple. The spin-orbit scattering amplitude is proportional to $\boldsymbol{\sigma}\cdot\mathbf{R}\times\boldsymbol{\Gamma}$. However, the radius vector $\mathbf{R}$ at A (Fig. 1) has the opposite sign from $\mathbf{R}$ at C. This introduces into the spin term an intrinsic phase difference of π between these two spectral points. So for odd L (say $L=1$) as we have seen, the factor $e^{-iM\varphi}$ gives a phase difference of π between A and C, but the spin-orbit effects produce another phase change of π, leaving A back in phase with C and yielding distributions like those for M even. The additional characterization of the $J=L-\frac{1}{2}$ by $L+1$ distributions and $J=L+\frac{1}{2}$ by $L-1$ is apparently a purely quantum mechanical effect that arises from the algebra of the spin functions. As yet we have not found any semiclassical picture to help in understanding it better.

We have presented a somewhat simplified version of a large-angle spin-dependent diffraction theory in the expectation that the rather simple qualitative results will provide insight into the mechanisms for the unusual effects we are trying to explain. If the general qualitative predictions of this article, and if the quantitative predictions of the more complete treatment of the model are corroborated by future experiments, deuteron stripping reactions as well as other direct reaction processes should become even more important than heretofore as a tool in nuclear spectroscopy, and further, the utilization of the unusual odd-even L behavior described here might prove fruitful in other fields.

ACKNOWLEDGMENTS

The author would like to thank Professor C. M. Sommerfield and Professor D. A. Bromley for stimulating discussions.

PHYSICAL REVIEW VOLUME 136, NUMBER 2B 26 OCTOBER 1964

Interaction of High-Energy Protons and Helium Ions with Niobium*†

RALPH G. KORTELING‡ AND EARL K. HYDE
Lawrence Radiation Laboratory, University of California, Berkeley, California

(Received 11 June 1964)

Production cross sections were measured radiochemically for isotopes of niobium, zirconium, copper, nickel, and sodium produced in niobium targets bombarded with 240, 320, 500, and 720 MeV protons and with 320, 500, 720, and 880 MeV helium ions. For the proton bombardments these cross sections were also calculated by the Monte Carlo method with an electronic computer by use of the conventional two-step model of high-energy reactions. Interpolated results of a previous calculation by Metropolis and co-workers were used to simulate the effect of the initial high-energy cascade. These results were used in turn as input data for an evaporation calculation. A comparison of the theoretical yields of final products with the observed yields indicates that the theory accounts fairly well for low-deposition-energy products (niobium and zirconium isotopes), and quite well for high-deposition-energy products (copper and nickel isotopes). The theory fails completely to account for the yields of sodium isotopes, whose production must be ascribed to fragmentation, as noted previously by others. No Monte Carlo calculations were made for helium-ion-induced reactions. However, a comparison of yields of products of helium-ion- and proton-induced reactions shows a remarkable similarity at all energies and for all products. The main difference is a greater yield by a factor of two in the case of helium-ion bombardments. The implications of this for the mechanism of fragmentation are discussed. During the course of this work a 15-min positron emitter was discovered and identified as Nb^{88}.

I. INTRODUCTION

ONE general method for the investigation of the interaction of high energy particles with complex nuclei is the radiochemical analysis of the heavy radioactive products of such interactions.[1] There exist many published studies of this type for a variety of targets bombarded with protons over the range of a few tens of MeV up to 27 GeV. The results have often been analyzed in terms of proposed mechanisms for the deposition of energy in the nucleus by the incident proton, and for the de-excitation of the excited nucleus by particle evaporation, by fission, or by fragmentation. There have

* This work was done under the auspices of the U. S. Atomic Energy Commission.

† Based on a thesis submitted by R. G. Korteling to the Department of Chemistry, University of California, Berkeley, California.

‡ Present address: Department of Chemistry, Carnegie Institute of Technology, Pittsburgh, Pennsylvania.

[1] See review article by J. M. Miller and J. Hudis, Ann. Rev. Nucl. Sci. 9, 159 (1959).

been many fewer experimental studies of the interaction of more complex projectiles such as deuterons or helium nuclei with complex nuclei, chiefly because most high-energy accelerators have been designed for the acceleration of protons only. In fact, there exist only two accelerators which are equipped to accelerate helium ions in the range of a few hundred MeV up to a maximum of about 900 MeV. These are the Berkeley 184-in. synchrocyclotron and the synchrocyclotron of the Joint Institute for Nuclear Research at Dubna in the Soviet Union.

The purpose of the investigation reported here was to carry out a careful study of the reaction products in a typical medium weight target element bombarded alternately with protons and with helium ions under similar experimental conditions and over the energy range of 240 to 880 MeV. The comparison of the results was expected to indicate similarities and differences in the interaction of the two types of particles, particularly in the first or energy deposition stage of the reaction. It was carried out as a companion study to one by Crespo, Hyde, and Alexander[2] in which the recoil and yield characteristics of the fragmentation products, Na^{24} and Mg^{28}, were measured in a series of targets bombarded with protons and helium ions over the same energy range.

A second purpose of the investigation was to check with some precision the predictions of a conventional two-step model of high-energy nuclear reactions induced by protons. In this model, as discussed in detail in the review article of Hudis and Miller,[1] the first step of the reaction is a prompt cascade of nucleon-nucleon collisions. These collisions are initiated by the incoming proton which converts a collection of target nuclei into a collection of struck nuclei with differing numbers of neutrons and protons and differing levels of excitation. The second step is the de-excitation of these excited nuclei by evaporation of neutrons, protons, deuterons and other particles. Monte Carlo methods of calculation of both stages of the reaction have been formulated in past publications by others. However, in only a few instances have these methods been applied in succession to the case of a specific target-projectile combination in order to make detailed predictions of expected reaction products. We have applied the Monte Carlo calculation method in succession to the two stages of the reactions induced in niobium by protons. Our results are useful both in indicating which parameters are the sensitive ones, particularly in the evaporation de-excitation stage, and in showing to what extent the two-step model is capable of explaining the cross-section results.

Niobium was selected as a target material for several reasons. It is monoisotopic and it contains sufficient nucleons for a meaningful calculation of the knock-on and evaporation cascades. Its spectrum of reaction products is not complicated by the presence of fission products. And, finally, it is available in metallic foils of convenient thickness and sufficient chemical purity.

In an ideal experiment of this nature, one would investigate all possible products. Limitations of time and effort led us to investigate only five elements among the numerous products. Isotopes of niobium and zirconium were studied as indicators of reactions in which only a few tens of MeV were deposited in the target. Isotopes of copper and nickel were chosen as indicators of reactions in which some hundreds of MeV of excitation were required. The element sodium was chosen as an indicator of fragmentation products.

We discuss in order the experimental methods, the experimental results, the Monte Carlo calculations, the comparison of experimental and theoretical results, and finally the comparison of the results from the helium-ion and proton-induced reactions.

II. EXPERIMENTAL PROCEDURES

A. Target and Monitoring Details

Thin niobium target foils were irradiated in the internal beam of the 184-in. synchrocyclotron of the Lawrence Radiation Laboratory. By use of different settings, it was possible to select bombardment energies in the range 240–720 MeV for protons and 320–880 MeV for helium ions. We chose the four energies 240, 320, 500, and 720 MeV for the proton experiments and 320, 500, 720, and 880 MeV for the helium-ion experiments. These energies are believed to be correct within an uncertainty of ± 10 MeV. The beam intensity was of the order of 0.5 μA.

Deuteron contamination of the helium-ion beam was considered to be small. It was certainly negligibly small for the majority of the bombardments, which were conducted days after the last previous use of the cyclotron for deuteron acceleration.

The target arrangement consisted of a stack of foils clamped together in a simple copper target holder which could be readily connected and removed from the internal cyclotron probe. The beam struck the outer edge of the foil stack at right angles to the target. Since the total stack thickness was small compared to the range of the particles, there was multiple traversal of the foils. In order of traversal by the beam, the stack consisted of a 3-mil aluminum guard foil, a 1-mil aluminum monitor foil (of $>99.99\%$ purity), a second 3-mil aluminum guard foil, and a 2.5-mil niobium foil. In the experiments in which sodium production was studied, guard foils of niobium enclosed the target foil to prevent extraneous activity from interfering with the measurement of sodium cross sections. The foils were cut to dimensions 2×3.5 cm and milled as a stack on all sides to insure uniform area. Special care was taken to maintain clean surfaces. Since the beam cuts a circular path outward, the alignment of the leading edge of the foil stack was critical. Hence, the machining of the leading edge was made after the stack was mounted in the

[2] V. P. Crespo, J. M. Alexander, and E. K. Hyde, Phys. Rev. 131, 1763 (1963).

target holder. Checks were made to establish the correctness of the alignment of the target and monitor foils, and the error due to misalignment was found to be below 1%.

The niobium used in all the irradiations came from the same 2.5-mil sheet, which when analyzed by optical spectroscopy gave the impurity values listed in Table I. The guard foils protected the monitor foil from any background activity resulting from any structural materials of higher Z.

The total proton current passing through the foil stack was determined by measurement of Na^{24} activity produced by the reaction, $Al^{27}(p,3pn)Na^{24}$. The cross section for this reaction is nearly constant over the energy range of interest here and from the careful work of many authors its value is well known.[3] We used a value of 9.5 mb at 240 MeV and of 10.6 mb at our three other bombardment energies.

The integrated helium-ion beam was monitored with the Na^{24} activity produced in the monitor foil by the reaction $Al^{27}(\alpha,\alpha 2pn)Na^{24}$. The excitation function for this reaction has been measured [4,5] only to 380 MeV. At 380 MeV it has the value 24 mb, and it decreases slowly at an unknown rate at higher bombarding energies. We use the value of 24 mb throughout the energy range 320 to 880 MeV. We also quote the ratio of our product cross section to the monitor cross section so that the correction to an absolute cross section value can easily be made later, when better values of the monitor cross section are available.

In some cases when the count rate of the Na^{24} activity in the monitor foils was too high for accurate determination, the longer lived Na^{22} was measured instead. The Na^{22} activity was then converted to an equivalent Na^{24} count rate by a conversion factor determined in a separate set of experiments.

TABLE I. Impurities in the niobium foil.

Impurity	Percent	Impurity	Percent
Oxygen	0.03	Titanium	0.01
Nitrogen	0.03	Tungsten	less than 0.01
Carbon	0.015	Zirconium	less than 0.005
Tantalum	0.05	Nickel	less than 0.005
Iron	0.015		

B. Chemical Separations

A short time after each irradiation, the niobium foil was dissolved in a mixture of hydrofluoric and nitric acids. Ten to twenty milligrams of zirconium, copper, nickel, and sodium were added to the solution, following which, radiochemical separations were performed to isolate one or more of the product elements of interest in high chemical and radiochemical purity. Outlines of the methods are given in Appendix A. The final chemical step for each element consisted of the precipitation of a compound of definite composition which was dried and weighed to determine the percentage recovery of the element. Errors in the determination of chemical yield were estimated to be less than 5%. The precipitate was filtered onto a glass filter disc to form a sample of approximately 8 mg/cm² thickness which was suitably mounted for measurement of its radioactivity.

C. Activity Measurements

The gamma spectrum of each element was measured with a sodium iodide crystal coupled to a multichannel

TABLE II. Decay properties of investigated nuclides.

Nuclide	Half-life	Rad.	Energy (MeV)	%	Nuclide	Half-life	Rad.	Energy (MeV)	%
Nb-90	14.7 h	β^+	1.50	50	Cu-64	12.88 h	β^-	0.573	38
		e^-	0.114	11			β^+	0.656	19
		e^-	0.123	19	Cu-61	3.32 h	β^+	0.56	3
Nb-89	1.79 h	β^+	2.86	91			β^+	0.94	5
Zr-89	79.3 h	β^+	0.90	30			β^+	1.15	1.1
		γ	0.915	100			β^+	1.21	53.1
Sr-87m	2.75 h	e^-	0.363	22	Ni-66	54.8 h	β^-	0.20	100
Zr-88	85 d	γ	0.394	100	Cu-66	5.10 min	β^-	1.59	9
		e^-	0.377	4.62			β^-	2.63	91
Y-88	105 d	β^+	0.57	0.7	Ni-65	2.56 h	β^-	0.60	23
Zr-87	1.57 h	β^+	2.10	83			β^-	1.01	8
Zr-86	17 h	γ	0.241	100			β^-	2.10	69
Y-86	14.6 h	β^+	0.90	3	Ni-57	36 h	β^+	0.849	39.9
		β^+	1.32	15			β^+	0.712	5.6
		β^+	1.41	5	Na-24	15 h	β^-	1.391	100
		β^+	2.09	6	Na-22	2.58 year	β^+	0.554	89.8
Y-87m	14 h	e^-	0.363	22					
Cu-67	61.6 h	β^-	0.395	45					
		β^-	0.484	35					
		β^-	0.577	20					
		e^-	0.083	≈20					

[3] See review article by J. B. Cumming, Ann. Rev. Nucl. Sci. **13**, 261 (1963).
[4] M. Lindner and R. N. Osborne, Phys. Rev. **91**, 342 (1953).
[5] W. E. Crandall, G. P. Millburn, R. V. Pyle, and W. Birnbaum, Phys. Rev. **101**, 329 (1956).

TABLE III. Product cross sections from proton bombardments of niobium.

240-MeV protons on niobium					320-MeV protons on niobium			
Cross section[a] (mb)	$\bar{X}$[b]	$\sigma_{\bar{x}}$[c]	D	Product	Cross section[a] (mb)	$\bar{X}$[b]	$\sigma_{\bar{x}}$[c]	D
65.6	6.90		1	Nb-90	54.8	5.17	0.50	2
25.0	2.63		1	Nb-89	21.7	2.05		1
62.7	6.60	2.5×10^{-2}	2	Zr-89	59.7	5.73		1
80.9	8.52		1	Zr-88	71.7	6.76		1
46.7	4.92		1	Zr-87	42.4	4.00		1
1.46×10^{-3}	1.54×10^{-4}	4.5×10^{-6}	2	Cu-67	5.20×10^{-3}	4.91×10^{-4}	2.5×10^{-5}	2
2.09×10^{-2}	2.20×10^{-3}	1.5×10^{-4}	2	Cu-64	0.103	9.75×10^{-3}	2.6×10^{-4}	2
5.18×10^{-3}	5.45×10^{-4}	6.2×10^{-5}	2	Cu-61	3.42×10^{-2}	3.23×10^{-3}	1.4×10^{-4}	2
1.03×10^{-4}	1.08×10^{-5}		1	Ni-66	3.80×10^{-4}	3.58×10^{-5}		1
5.50×10^{-4}	5.79×10^{-5}		1	Ni-65	3.15×10^{-3}	2.97×10^{-4}		1
3.49×10^{-4}	3.67×10^{-5}		1	Ni-57	1.77×10^{-3}	1.67×10^{-4}		1
8.21×10^{-3}	8.64×10^{-4}		1	Na-24	1.48×10^{-2}	1.40×10^{-3}	4.0×10^{-5}	2
1.92×10^{-2}	2.04×10^{-3}	1.3×10^{-4}	2	Na-22	1.59×10^{-2}	1.50×10^{-3}	1.9×10^{-4}	2
500-MeV protons on niobium					720-MeV protons on niobium			
Cross section[a] (mb)	$\bar{X}$[b]	$\sigma_{\bar{x}}$[c]	D	Product	Cross section[a] (mb)	$\bar{X}$[b]	$\sigma_{\bar{x}}$[c]	D
47.4	4.47	0.24	2	Nb-90	37.0	3.49	0.35	2
17.7	1.67		1	Nb-89	13.9	1.31		1
44.8	4.23	2.5×10^{-2}	2	Zr-89	38.5	3.63		1
54.2	5.11		1	Zr-88	42.1	3.97		1
32.8	3.09		1	Zr-87	26.1	2.46		1
2.94×10^{-2}	2.77×10^{-3}	1.6×10^{-5}	2	Cu-67	0.119	1.12×10^{-2}	4.7×10^{-4}	3
0.731	6.90×10^{-2}	3.4×10^{-3}	2	Cu-64	2.79	0.263	1.3×10^{-2}	3
0.416	3.92×10^{-2}	3.5×10^{-3}	2	Cu-61	1.73	0.163	1.0×10^{-2}	3
2.86×10^{-3}	2.70×10^{-4}	3.5×10^{-6}	2	Ni-66	8.30×10^{-3}	7.83×10^{-4}	1.5×10^{-5}	2
2.20×10^{-2}	2.08×10^{-3}	1.3×10^{-4}	2	Ni-65	6.28×10^{-2}	5.92×10^{-3}	1.0×10^{-5}	2
1.83×10^{-2}	1.73×10^{-3}	1.5×10^{-4}	2	Ni-57	7.30×10^{-2}	6.89×10^{-3}	3.5×10^{-5}	2
4.27×10^{-2}	4.03×10^{-3}	1.2×10^{-4}	2	Na-24	0.130	1.23×10^{-2}	1.0×10^{-4}	2
2.57×10^{-2}	2.42×10^{-3}	1.0×10^{-4}	2	Na-22	7.29×10^{-2}	6.88×10^{-3}	9.0×10^{-5}	2

[a] Na^{24} monitor cross section taken as 9.5 mb for 240-MeV protons, and as 10.6 mb for 320-, 500-, and 720-MeV protons.
[b] $\bar{X}$=ratio of product cross section to Na^{24} monitor cross section.
[c] $\sigma_{\bar{x}}$=standard error of X when number of determinations D is greater than 1.

pulse-height analyzer. These spectra served to identify the isotopes present in the sample, to reveal possible impurities, and, in some cases, to calibrate the counting efficiency of the beta counters. All quantitative yield measurements were made by an analysis of decay curves of the activity measured in methane-flow end-window proportional counters. These counters were standardized for absolute counting in cooperation with Blann[6] by the procedure published by Bayhurst and Prestwood.[7]

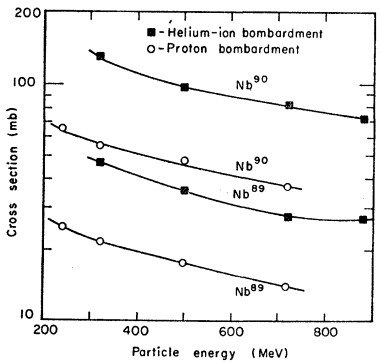

FIG. 1. Production cross section of niobium isotopes in niobium targets bombarded with high-energy protons (shown by circles) and high-energy helium ions (shown by squares).

[6] H. M. Blann, University of California, Lawrence Radiation Laboratory report, UCRL-9190, May 1960 (unpublished).
[7] B. P. Bayhurst and R. J. Prestwood, Nucleonics **17**, 82 (1959).

According to this method, an empirical relationship between the efficiency of the counter and the average beta energy is used to determine the counting efficiency for a particular activity. Independent empirical corrections for self-absorption, back scattering, etc., were not made. We estimate an absolute error of 5 to 10% on our standardization of counting efficiency. However, since our samples are measured relative to the Na^{24} monitor activity standardized by the same method, the resultant error in the reported cross sections is somewhat less.

Errors in determination of the count rate were less than 2% and in the resolution of the decay curves into components less than 3%. Errors in the correction for the decay scheme varied for each nuclide. The values which we used[8,9] are listed in Table II.

For any of our reported absolute cross sections we estimate an over-all error of 20%.

Details of the analysis of activity measurements for individual elements are given in Appendix B.

[8] *Nuclear Data Sheets*, compiled by K. Way *et al.* (Printing and Publishing Office, National Academy of Sciences—National Research Council, Washington 25, D. C.).
[9] D. Strominger, J. M. Hollander, and G. T. Seaborg, Rev. Mod. Phys. **30**, 583 (1958).

TABLE IV. Product cross sections from helium-ion bombardments of niobium targets.

320-MeV helium ions on niobium					500-MeV helium ions on niobium			
Cross section[a] (mb)	$\bar{X}$	$\sigma_{\bar{x}}$	D	Product	Cross section[a] (mb)	$\bar{X}$	$\sigma_{\bar{x}}$	D
129	5.37	0.27	2	Nb-90	97.2	4.05	0.31	2
46.8	1.95		1	Nb-89	35.5	1.48		1
111	4.61		1	Zr-89	81.4	3.39	3.0×10^{-2}	
145	6.04		1	Zr-88	105	4.38		1
92.2	3.84		1	Zr-87	65.8	2.74		1
1.08×10^{-2}	4.49×10^{-4}	1.0×10^{-5}	3	Cu-67	7.15×10^{-2}	2.98×10^{-3}	1.6×10^{-4}	3
0.173	7.19×10^{-3}	8.3×10^{-4}	3	Cu-64	0.145	6.05×10^{-2}	1.7×10^{-3}	3
4.42×10^{-2}	1.84×10^{-3}	7.0×10^{-5}	3	Cu-61	6.50×10^{-1}	2.71×10^{-2}	1.0×10^{-3}	3
1.06×10^{-3}	4.40×10^{-5}		1	Ni-66	7.30×10^{-3}	3.04×10^{-4}		1
6.07×10^{-3}	2.53×10^{-4}		1	Ni-65	4.08×10^{-2}	1.70×10^{-3}		1
5.40×10^{-3}	2.25×10^{-4}		1	Ni-57	3.60×10^{-2}	1.50×10^{-3}		1
4.32×10^{-2}	1.80×10^{-3}		1	Na-24	0.113	4.70×10^{-3}		1
4.68×10^{-2}	1.95×10^{-3}		1	Na-22	8.64×10^{-2}	3.60×10^{-3}		1

720-MeV helium ions on niobium					880-MeV helium ions on niobium			
Cross section[a] (mb)	$\bar{X}$	$\sigma_{\bar{x}}$	D	Product	Cross section[a] (mb)	$\bar{X}$	$\sigma_{\bar{x}}$	D
83.5	3.48	0.10	2	Nb-90	72.2	3.01	0.15	3
27.8	1.16		1	Nb-89	27.1	1.13	6.0×10^{-2}	2
73.9	3.08		1	Zr-89	63.1	2.63		1
93.1	3.88		1	Zr-88	79.7	3.32		1
55.9	2.33		1	Zr-87	47.8	1.99		1
0.166	6.91×10^{-3}	2.6×10^{-4}	2	Cu-67	0.257	1.07×10^{-2}	9.8×10^{-4}	4
4.34	0.181	3.5×10^{-3}	2	Cu-64	6.26	0.261	9.6×10^{-3}	4
2.59	0.108	2.0×10^{-3}	2	Cu-61	4.75	0.198	1.4×10^{-2}	4
1.92×10^{-2}	8.02×10^{-4}		1	Ni-66	2.86×10^{-2}	1.19×10^{-3}	6.1×10^{-5}	3
0.121	5.06×10^{-3}		1	Ni-65	0.167	6.97×10^{-3}	4.2×10^{-4}	3
0.143	5.96×10^{-3}		1	Ni-57	0.242	1.01×10^{-2}	8.3×10^{-4}	3
0.300	1.25×10^{-2}		1	Na-24	0.533	2.22×10^{-2}		1
0.196	8.18×10^{-3}		1	Na-22	0.254	1.06×10^{-2}	1	1

[a] Na^{24} monitor cross section taken as 24 mb for all energies.

III. EXPERIMENTAL RESULTS

The experimental cross sections are listed in Tables III and IV in blocks according to bombarding energy. In all cases, both the absolute cross section and the ratio of the cross section for the isotope to that for the Na^{24} yield in the aluminum monitor are given. Each block contains the average value of the determined ratios under $\bar{X}$. When more than one measurement was made, a standard error is given under the heading $\sigma_{\bar{x}}$ and the number of determinations under D. The absolute cross section was computed from the average values by use of the Na^{24} monitor cross sections listed in the tables. It is emphasized again that the Na^{24} monitor cross section of 24 mb for helium-ion induced reactions is an estimate and may be progressively incorrect (on the high side) as the helium-ion energy increases.

The results are also displayed graphically in Figs. 1 through 5.

IV. MONTE CARLO CALCULATIONS OF PRODUCT YIELDS

In this section, we discuss the calculation of reaction product yields on the assumption of the validity of the conventional two-step model.

For the first stage we have used selected results of Metropolis and co-workers[10] to determine the spectrum of struck nuclei and their excitation energies at the end of the prompt cascade. The detailed assumptions and mechanics of the calculation are given in the Metropolis paper so we need only mention some of the main points.

The target nucleus was represented by a degenerate Fermi gas in a square-well potential of radius 1.3×10^{-13} $A^{1/3}$ cm. The incoming proton was assumed to make a

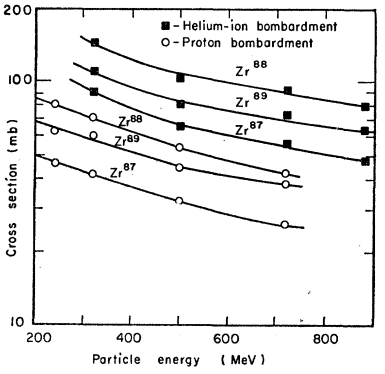

FIG. 2. Production cross sections of zirconium isotopes in niobium targets bombarded with high-energy protons (shown by circles) and high-energy helium ions (shown by squares).

[10] N. Metropolis, R. Bivens, M. Strom, A. Turkevich, J. M. Miller, and G. Friedlander, Phys. Rev. **110**, 185 (1958); **110**, 204 (1958).

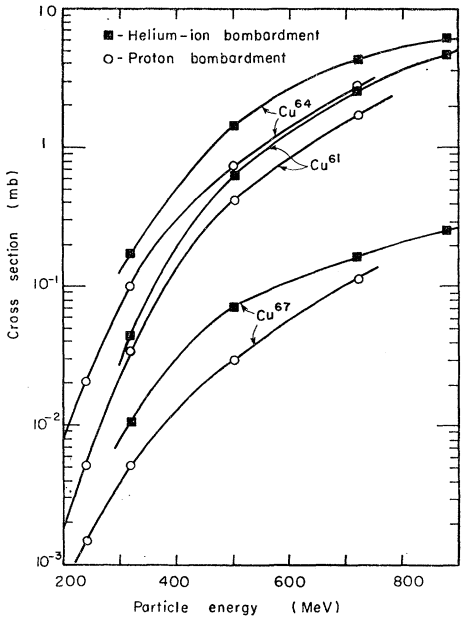

FIG. 3. Production cross sections of copper isotopes in niobium targets bombarded with high-energy protons (shown by circles) and high-energy helium ions (shown by squares).

collision with one nucleon in the well. After the collision, if both particles had a final energy greater than the maximum Fermi energy, the collision was allowed; if not, the collision was rejected as unphysical. After the initial collision, both particles were followed separately by Monte Carlo calculations to see whether they made additional collisions before they emerged from the

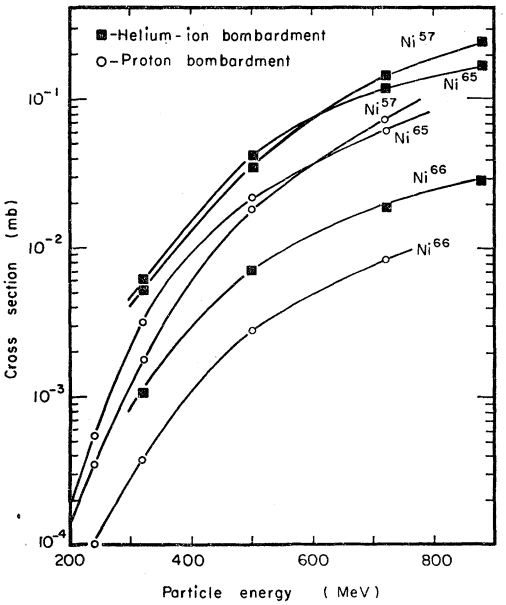

FIG. 4. Production cross sections of nickel isotopes in niobium targets bombarded with high-energy protons (shown by circles) and high-energy helium ions (shown by squares).

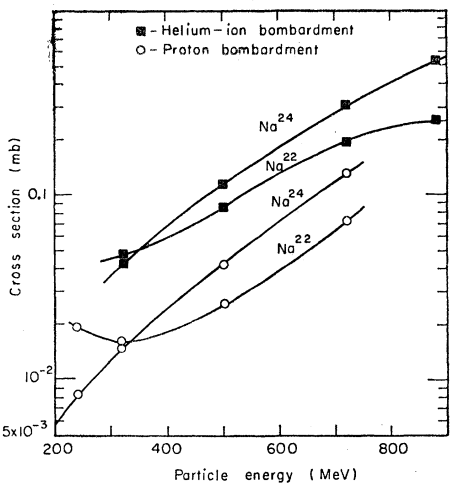

FIG. 5. Production cross sections of sodium isotopes in niobium targets bombarded with high-energy protons (shown by circles) and high-energy helium ions (shown by squares).

nucleus. When all collision partners had either escaped from the nucleus or been absorbed, a summation was made of the energy of the "holes" in the Fermi gas and the excitation energy of the bound collision partners. The output information consisted of summaries of the following information: (1) the type, number, energy, and angular distribution of emitted particles; (2) the type, number, and excitation energy of all residual (struck) nuclei.

Metropolis *et al.*[10] did not use niobium as a target in their calculations, but they did consider Ru^{100} which is not much different in composition. We have used their results for Ru^{100} and "transposed" them for the Nb^{93} case by subtracting three units of charge and seven units of mass from each of the residual nuclei at the end of the cascade. This transposition was performed for the three energies of 462, 944, and 1844 MeV, although the third energy falls above the energy range

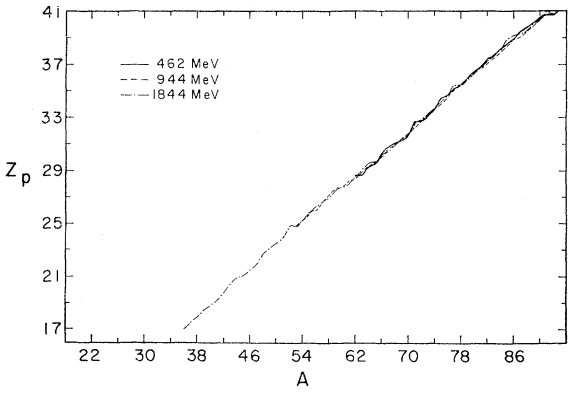

FIG. 6. Variation in calculated value of most probable nuclear charge Z_p with mass number of reaction product. Niobium target bombarded with protons. Data are for $a=A/20$ and the emission of six types of particles.

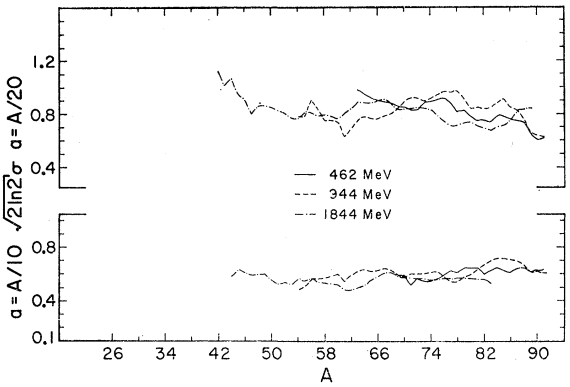

FIG. 7. Width of the distribution in charge of the final products as a function of mass number. Calculated value of averaged Gaussian half-widths at half-maximum, $(2\ln 2)^{1/2}\sigma$, for niobium targets bombarded with protons. Results shown for two values of the evaporation parameter: $a=A/20$ and $a=A/10$.

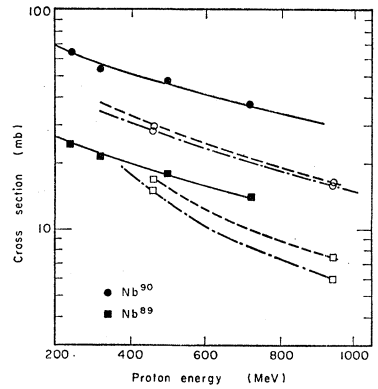

FIG. 9. Experimental production cross sections for niobium isotopes (solid symbols) compared to calculated values (open symbols). Broken curve indicates trend of calculated results for evaporation parameter $a=A/10$; dot-dash curve shows trend for $a=A/20$.

used in our experimental work and will not be discussed in detail.

The transposed output data of the prompt cascade were used as the input information of a Monte Carlo evaporation cascade calculation. We followed closely the calculation outlined by Dostrovsky, Fraenkel, and Friedlander,[11] which, in turn, is based upon the theoretical ideas of Weisskopf.[12] Dostrovky *et al.* used the WEIZAC computer at the Weizmann Institute. We used a program written for the IBM 7090 by Alexander, Altman, and Howry.[13]

The level density expression is of crucial importance to any evaporation calculation based on the Weisskopf theory. Dostrovsky, Fraenkel, and Friedlander[11] chose the form

$$W(E)=C\exp\{2[a(E-\delta)]^{1/2}\},$$

where C is a constant, a is a constant proportional to mass number, E is the energy, and δ is a correction term to adjust for odd-even pairing energy effects. The term δ, in effect, adjusts the position of the ground-state energy and was evaluated from Cameron's[14] semi-empirical mass equation. We used the values $A/20$ and $A/10$ for the parameter a.

All the constants required for solution of the evaporation equations were read into the computer. The atomic number and mass, the excitation energy, and the number of cases to be examined were specified. A random number selected the particles to be emitted from a distribution weighted by the relative emission probability for each particle. The weighting fractions were recomputed at each step of the evaporation chain. Other random numbers selected the kinetic energy of the particle from the calculated kinetic energy distributions. This information determined the result of the first evaporation step and the input data for the next step. The procedure was repeated until insufficient excitation energy remained to evaporate any particle. The com-

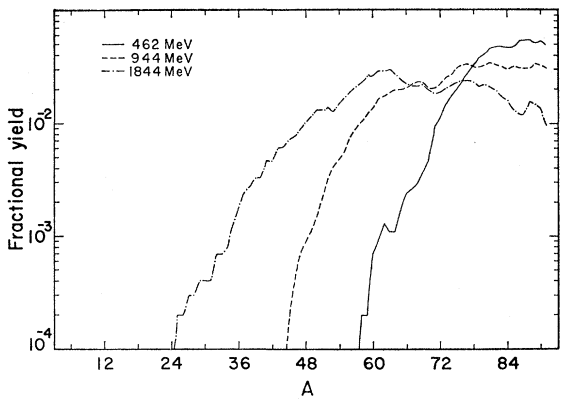

FIG. 8. Averaged mass-yield curve from the Monte Carlo cascade-evaporation calculation for reaction of protons with niobium. Data are for $a=A/20$ and the emission of six types of particles.

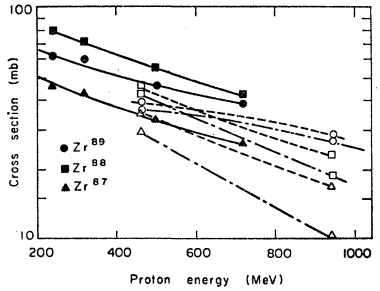

FIG. 10. Experimental production cross sections for zirconium isotopes (solid symbols) compared to calculated values (open symbols). Broken curve indicates trend of calculated results for evaporation parameter $a=A/10$; dot-dash curve shows trend for $a=A/20$.

[11] I. Dostrovsky, Z. Fraenkel, and G. Friedlander, Phys. Rev. **116**, 683 (1959).
[12] V. Weisskopf, Phys. Rev. **52**, 295 (1937).
[13] J. M. Alexander, L. Altman, and S. Howry, Lawrence Radiation Laboratory, 1962 (unpublished).
[14] A. G. W. Cameron, Atomic Energy of Canada Ltd. report CRP-690, 1957 (unpublished); Can. J. Phys. **35**, 1021 (1958).

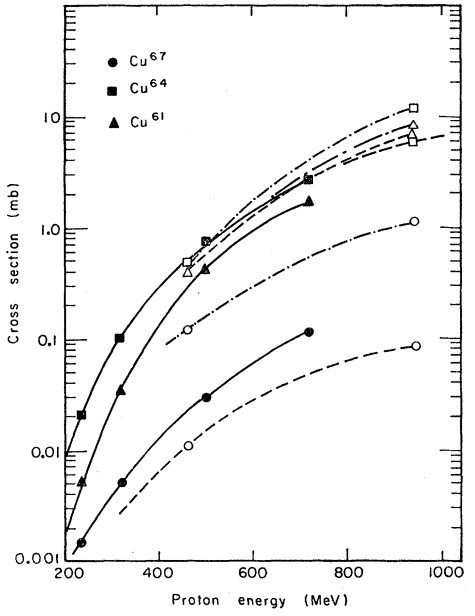

FIG. 11. Experimental production cross sections for copper isotopes (solid symbols) compared to calculated values (open symbols). Broken curve indicates trend of calculated results for evaporation parameter $a=A/10$; dot-dash curve shows trend for $a=A/20$.

puter then was instructed to move on to the next evaporation chain. The information obtained from each evaporation chain was (1) the type, number, and energy of emitted particles; (2) the type, number, and residual excitation energy of the final products; (3) the detailed evaporation path. For our purposes, only certain summaries of this information were useful and statistically reliable. The chief summary needed for comparison with experimental data was a table of the final products, giving for each product the Z, A, number of cases, and fraction of the total products.

In most of our calculations we limited the evaporation to the following six particles: neutron, proton, deuteron, triton, helium-3 nucleus, and helium-4 nucleus. In a few test calculations, the evaporation of heavier particles, numbering 16 in all, was permitted. We did not find that this change made an appreciable difference in the yield of the products in which we were interested.

The input information from the Metropolis *et al.* cascade calculations covered 809 cases at 462 MeV and 695 cases at 944 MeV. The geometric cross section for protons interacting with niobium is ≈ 1200 mb. Hence, the statistical error for any final product with a formation cross section less than a few millibarns was quite large. To reduce somewhat the statistical error in the results five evaporation calculations were performed for each initial cascade case. It also proved helpful to employ certain averaging procedures to smooth out the results. This is possible and proper since the model predicts systematic trends in yield as a function of atomic mass and charge. For example, the isobaric distribution could be approximated by a Gaussian curve. The computer results for three or more products of different Z at each value of A could be plotted on probability paper to determine a most probable Z, designated Z_p, and the standard deviation σ of the Gaussian distribution. Resulting values for Z_p and σ are shown in Figs. 6 and 7. In order to obtain a satisfactorily smooth curve of fractional yield versus mass number, it was necessary to average the isobaric yields over 3 mass units. Figure 8 shows one summary of our calculations averaged in this fashion.

With the aid of our curves for Z_p, the charge distribution parameter σ, the isobaric yield curves, and a total cross section value of 1230 mb, obtained by graphical interpolation of the results of Gooding,[15] we were able to calculate the cross section of any isotope. We made such calculations for the isotopes isolated in our work. We discuss these in the next section.

Details of the calculations and the results are given more fully in the thesis study by one of us.[16]

V. COMPARISON OF THE EXPERIMENTAL AND CALCULATED CROSS SECTIONS

Figures 9–12 show the calculated yields at two bombarding energies and the experimental yields at four for the isotopes of niobium, zirconium, copper, and nickel studied in our experiments.

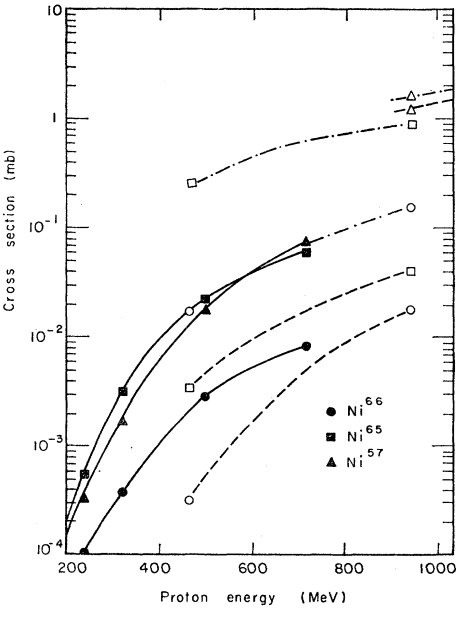

FIG. 12. Experimental production cross sections for nickel isotopes (solid symbols) compared to calculated values (open symbols). Broken curve indicates trend of calculated results for evaporation parameter $a=A/10$; dot-dash curve shows trend for $a=A/20$.

[15] T. J. Gooding, Nucl. Phys. **12**, 241 (1959).

[16] R. G. Korteling, University of California, Lawrence Radiation Laboratory, report UCRL-10461, 1962 (unpublished).

A. Low-Deposition-Energy Processes

The niobium and zirconium results are representative of low-deposition-energy processes. The experimental and calculated values are compared in Figs. 9 and 10. The excitation functions have a negative slope in agreement with the expectation that their maximum cross sections are obtained at much lower bombarding energies than those considered here. This decrease can be attributed to the competition from processes of higher deposition energy as the bombarding energy is increased. The fact that the yields decrease rather slowly is proof that the prompt cascades include a sizeable proportion of events in which only a small fraction of the energy of the incoming particle is transferred to the target nucleus. The rough agreement of the experimental and theoretical curves shows that the general trend with increasing energy is correctly reproduced.

The calculation underestimates the measured value for Nb^{90} by a factor of 1.7 at 462 MeV and by a larger factor at higher bombarding energies. The agreement for Nb^{89} is satisfactory at 462 MeV but worsens at higher energies. These discrepancies are of the same order as those observed by others for products of the (p,pxn) type when x is a small number.[10,17–20] The comparison of calculated and experimental values for the zirconium isotopes is somewhat better. At 462 MeV the calculation underestimates the values for Zr^{88} and Zr^{89} by about 25%. The experimental value for Zr^{87} is bracketed by the calculated values based on $A/20$ and $A/10$ for the level density parameter a. There is a gradual worsening of this agreement at higher energies.

B. High-Deposition-Energy Processes

The experimental cross sections for copper and nickel isotopes show sharply increasing excitation functions. The slopes of these curves are greater for the more neutron-deficient isotopes than for the neutron-excess isotopes. These are the qualitative properties expected from the cascade-evaporation model. The quantitative predictions of the model are presented in Figs. 11 and 12 and compared with the experimental data.

The agreement in most of the cases can be considered excellent both for the order of magnitude for these small-yield products, and for the slope of the excitation functions. In the cases of Cu^{64}, Cu^{67}, Ni^{66}, and Ni^{65}, the theoretical curves for the two choices of the a parameter in the level density formula bracket the experimental results. In the case of the very light product Cu^{61} the calculation overestimates the yield, but by less than a factor of 2, which is not serious. The lightest nickel isotope, Ni^{57}, is an exception. It is badly overestimated by the calculation.

We conclude that within the statistical accuracy imposed by the limited number of cascade events considered in the calculation, the yields of the copper and nickel isotopes on the neutron-excess side of beta stability are satisfactorily described by the conventional reaction model. The yields could easily be more closely calculated by an adjustment of the level density parameter within a reasonable range of choices. These cases represent large deposition energy (300 MeV or more on the average) sufficient for the removal of about 30 units of mass from the target nucleus. The fact that the neutron-deficient isotopes of these elements are not so well calculated may indicate that the charge distribution of yields is improperly estimated.

C. High-Deposition-Energy Processes Leading to Fragmentation

The production cross sections for Na^{24} and Na^{22} (see Fig. 5) increase with bombarding energy. Our results follow the systematic trends observed for the production of Na^{24} in other targets by Caretto, Hudis, and Friedlander,[21] and by Crespo, Alexander, and Hyde.[2] Our experimental data for Na^{22} are considerably less certain than those for Na^{24} and, in particular, the higher yield of Na^{22} at 240 than at 320 MeV is questionable.

Two features of the excitation functions may be mentioned. First, the slopes are not as great as those for the copper and nickel isotopes; there is only a factor of 10 increase in yield over the range of bombarding energy compared to a factor of about 100 for the copper and nickel isotopes. Second, the ratio of the more neutron-deficient Na^{22} isotope to Na^{24} decreases with increasing bombarding energy, whereas the corresponding ratios for the copper and nickel isotopes increase. Both these observations are contrary to the predictions of the reaction model which would say that the slope of the excitation function and the increasing yield of neutron-deficient over neutron-excess products should be much greater for sodium than for copper and nickel.

Furthermore, the yields of the sodium isotopes are orders of magnitude greater than the cascade-evaporation model would predict. The experimental cross sections are comparable to those for copper and higher than those for nickel, whereas the calculation does not predict the formation of any products with mass <35 until the bombarding energy is raised above 1 GeV.

We conclude that the sodium isotopes were produced by a reaction mechanism quite distinct from that described by the conventional model, which is based on the evaporation of numerous small particles from a highly excited target nucleus. Our result supports the

[17] I. M. Ladenbauer and L. Winsberg, Phys. Rev. **119**, 1368 (1960).
[18] S. S. Markowitz, F. S. Rowland, and G. Friedlander, Phys. Rev. **112**, 1295 (1958).
[19] M. A. Caretto and G. Friedlander, Phys. Rev. **110**, 1169 (1958).
[20] N. T. Porile, Phys. Rev. **125**, 1379 (1962); N. T. Porile and S. Tanaka, Phys. Rev. **132**, 397 (1963).
[21] A. A. Caretto, J. Hudis, and G. Friedlander, Phys. Rev. **110**, 1130 (1958).

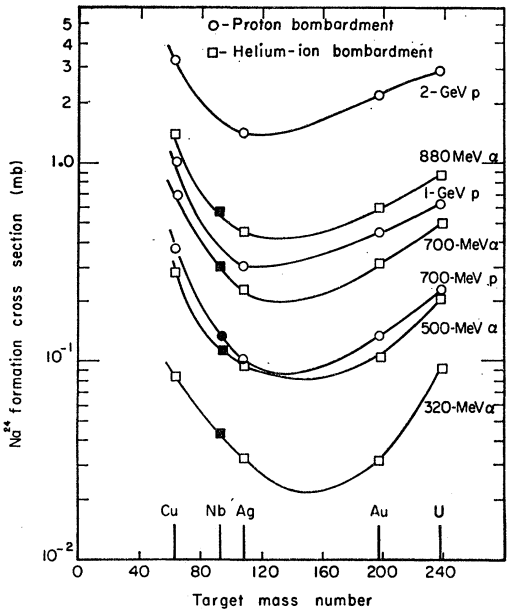

FIG. 13. Formation cross section for Na^{24} as a function of mass of target for proton and helium-ion induced reactions. Niobium points are from this work. The data at 1 and 2 GeV are from Caretto, Hudis, and Friedlander (see Ref. 21). The rest are from Crespo, Alexander, and Hyde (see Ref. 2). Proton data are given by circles, helium-ion data by squares. The niobium points are solid.

conclusion reached by many others[1,2,21–25] that an additional mechanism, often called fragmentation, is operative in reactions induced by particles of high energy.

It is interesting to compare our Na^{24} cross sections with those obtained by others from various targets; such a comparison is presented in Fig. 13. It can be seen that the points for niobium targets correlate with those for other elements. The unusual form of the curves in this figure constitutes part of the evidence for a fragmentation origin for Na^{24} as is discussed by Caretto, Hudis, and Friedlander[21] and Crespo, Alexander, and Hyde.[2]

VI. DISCUSSION OF RESULTS FOR REACTIONS INDUCED BY HELIUM IONS

The yields of the products for the helium-ion-induced reactions are listed in Tables III and IV and plotted in Figs. 1 through 5. The two striking features of the comparison of these yields to those obtained in the proton-induced reactions are the greater yields in the reactions induced by helium ions and the close parallelism of the excitation functions. The yield ratios are summarized in Table V. These ratios are close to the value 2 for all products and all bombarding energies. This is a striking constancy considering the great range of cross section values and the differences in slope for the different products. It seems apparent that the pattern of energy deposition is quantitatively very much the same in the helium-ion bombardments as it is in the proton bombardments.

This is an unexpected result for several reasons. We cite the conclusion from our discussion above and from the previous work of others that the sodium isotopes are formed by a reaction mechanism which is different from that which leads to the production of the heavier products. It seems surprising that the results for both types of reactions should be so similar for the two types of particles. This is particularly so if one accepts the fragmentation mechanism suggested by Wolfgang *et al.*[22] in which pion formation plays a significant role in transferring large amounts of energy to the struck nucleus. It seems unlikely that an alpha particle would produce pions in nearly the same yield as protons. It is usually stated that a pion can be produced only by the interaction of an individual nucleon with a nucleon in the target nucleus. Each component nucleon of the alpha particle has about one-quarter the total energy of the alpha particle, with a distribution related to the internal momentum. Since the cross section for pion production by a free nucleon is a steep function of energy in the region 100–500 MeV, one would expect fewer pions produced by alpha particles than by protons of the same energy over the range of energies we have studied. The threshold and the steep rise in the meson excitation function should be displaced to higher helium-ion energies. This difference in the ability of the two projectiles to produce mesons should be reflected in the production cross sections of products whose formation is influenced in a significant way by meson production and reabsorption. We see no evidence for differences in the production of any of the studied isotopes except that the yields are *higher* by a factor of 2 in the helium-ion experiments.

TABLE V. Ratio of the cross sections from helium-ion bombardments to those from proton bombardments.

Nuclide	320 MeV	500 MeV	720 MeV	Average
Nb-90	2.33	2.03	2.24	2.20
Nb-89	2.13	1.99	1.99	2.04
Zr-89	1.84	1.80	1.90	1.85
Zr-88	2.01	1.92	2.19	2.04
Zr-87	2.15	1.99	2.12	2.09
Cu-67	2.05	2.42	1.38	1.95
Cu-64	1.65	1.97	1.54	1.72
Cu-61	1.28	1.55	1.49	1.44
Ni-66	2.76	2.53	2.29	2.53
Ni-65	1.91	1.83	1.92	1.89
Ni-57	3.03	1.94	1.94	2.29
Na-24	2.89	2.62	2.29	2.60
Na-22	2.92	3.34	2.27	2.84
Average	2.23	2.15	1.97	

[22] R. Wolfgang, E. W. Baker, A. A. Caretto, J. B. Cumming, G. Friedlander, and J. Hudis, Phys. Rev. **103**, 394 (1956).
[25] J. B. Cumming, S. Katcoff, N. T. Porile, S. Tanaka, and A. Wyttenbach, Phys. Rev. **134**, B1262 (1964).
[24] N. A. Perfilov, O. V. Lozhkin, and V. P. Shamov, Usp. Fiz. Nauk **60**, 3 (1956) [English transl.: Soviet Phys.—Uspekhi **3**, 1 (1960)].
[25] J. B. Cumming, R. J. Cross Jr., J. Hudis, and A. M. Poskanzer, Phys. Rev. **134**, B167 (1964).

One might argue that the alpha particle compensates for its lesser pion production and reabsorption by initiating a more complex cascade with its four nucleons. This could well be true but it seems unlikely to us that this compensation should be so close for each of the four bombarding energies and for each group of products.

It is not possible to program a Monte Carlo calculation for the initial fast cascade induced in target nuclei struck by energetic helium nuclei because of insufficient data on elastic and inelastic cross sections of helium ions interacting with nucleons. In particular, the literature does not contain extensive data on the production cross sections for mesons in targets bombarded with helium ions. Another uncertainty is the fate of the helium ion after the first collision. Does it break up and release four fast nucleons in the interior of the target nucleus to propagate separate cascades, or does it retain its identity throughout the cascade until it is absorbed or escapes from the nucleus? There is some evidence that the latter is the case, at least for reactions occurring in the surface. Igo, Hansen, and Gooding[26] studied the $(\alpha,2\alpha)$ reaction in a series of targets bombarded at 910 MeV. They used two particle detectors to measure the identity, energy, and angle of the two alpha particles emerging from the target. Their results indicate a strong probability for alpha clusters in the nuclear surface and for a quasifree elastic collision of the incoming α particle with an alpha cluster.

The near constant value of 2 (Table V) in the ratios of yields in the helium-ion and proton experiments is caused, for the most part, by the larger reaction cross section for the helium ions. Huizenga and Igo[27] give 1628 mb as the reaction cross section for 46-MeV helium ions interacting with a niobium target. For the proton bombardment calculations we have used a value of 1230 mb interpolated from the measurements of Gooding[15] at 34 MeV. These values differ by 32%. It could easily be that the total inelastic cross sections for incident particles of 320–720-MeV energy are appreciably different from these determined at 46 and 34 MeV by these authors. It is known, for example, that there exists an approximate 15% nuclear transparency effect for a target with a mass in the region of niobium bombarded with protons in the energy range of 150 to 400 MeV. Nuclear transparency is probably not so pronounced for helium ions. However, no experimental measurements exist for the total reaction cross section for targets near niobium bombarded with protons and helium ions at these energies.

It is appropriate here to call attention to two other recent studies of spallation reactions with high-energy helium ions and protons. Miller[28] has compared the (p,pn) and $\alpha,\alpha n)$ reactions on Co^{59} targets with protons and helium ions in the same energy range used by us. He finds a marked similarity in the results. Winsberg[29] has studied the properties of the alpha-emitter Tb^{149} produced in the bombardment of tantalum and gold targets with protons ranging from 0.45 to 6.2 GeV and with helium ions of 0.5, 0.7, and 0.88 MeV. This is about 30 mass units removed from the tantalum target and hence can be compared, at least roughly ,with our copper and nickel products for niobium targets. This study agrees with ours in that the experimental excitation function is the same in the proton and helium-ion bombardments. However, Winsberg's analysis of his data on the recoil properties of the Tb^{149} product led him to conclusions about the reaction mechanism which are somewhat different from the conventional two-step mechanism based on the Monte Carlo calculations cited in this paper.

CONCLUSION

The comparison of our experimental results for proton-induced reactions with detailed calculations based on the conventional two-stage model of high-energy reactions shows that a wide variety of products produced by low- and high-energy transfers are moderately well described by the model. However, there is one group of products (the sodium isotopes) which require a separate mechanism (fragmentation).

The results for the helium-ion reaction are remarkably similar to the proton results for all groups of products indicating that the energy deposition process is nearly the same. Together with the study of Na^{24} fragmentation products reported by Crespo, Alexander, and Hyde,[2] our results indicate that fragmentation induced by helium ions is closely similar to that induced by protons. This result raises some unresolved questions about the high-energy cascade in reactions leading to fragmentation.

ACKNOWLEDGMENTS

We wish to acknowledge the interest and support of Professor I. Perlman in this work. Dr. John M. Alexander contributed many helpful suggestions on the evaporation program and provided us with much of the detailed input information. We are also grateful to him for discussions of the results. Lawrence L. Altman gave us invaluable help in the adaptation of the evaporation program to the needs of our study. We are grateful to Herbert C. Albrecht for the conversion of the initial cascade data to a form acceptable by the evaporation program. The assistance of the 184-in. cyclotron operating crew and of the Health Chemistry Group in conducting the bombardments is appreciated. We thank the analytical chemistry group for help in the analysis of our final samples.

[26] G. Igo, L. F. Hansen, and T. J. Gooding, Phys. Rev. **131**, 337 (1963).
[27] J. R. Huizenga and G. Igo, Nucl. Phys. **29**, 462 (1962).
[28] L. Miller, thesis, Department of Chemistry, University of California, Davis, California, 1964 (unpublished).
[29] L. Winsberg, Phys. Rev. **135**, B1105 (1964).

APPENDIX A. CHEMICAL PROCEDURES

Preliminary Steps. The foils[30] were snipped from the target after the irradiations to produce a uniform set of foils. After the niobium and aluminum pieces were weighed, the niobium foil was placed in a cellulose nitrate tube and the aluminum foil was stored for later mounting and counting. A cellulose nitrate tube was used for the dissolution of the niobium rather than glass because a corrosive mixture of concentrated hydrofluoric and nitric acids was employed to dissolve the niobium. After complete dissolution, the excess fluoride ion was removed by successive precipitation of calcium fluoride and barium fluorozirconate. These precipitates were removed by centrifugation and the supernatant solution was transferred to glass equipment. To this point the chemical treatment was the same for each case.

Niobium Separation Procedure. Niobium pentoxide was precipitated from the above target solution by digestion with potassium bromate in a water bath. The oxide was washed with a solution of dilute nitric acid and ammonium hydroxide, transferred to a cellulose nitrate tube, and dissolved in concentrated hydrofluoric acid. After a barium fluorozirconate precipitation, niobium pentoxide was precipitated with concentrated ammonium hydroxide, washed with a dilute solution of ammonium and sodium hydroxide, and dissolved by digestion with nitric and oxalic acids. A second acid precipitation of niobium pentoxide was carried out on an aliquot of the solution by adding potassium bromate and heating the solution. The niobium pentoxide was filtered through a weighed paper filter and washed with water, alcohol, and acetone. The sample was weighed and mounted in this form. After counting the sample, the precipitate was ignited and weighed to determine the chemical yield. The procedure took approximately 40 min.

Zirconium Separation Procedure. Twenty mg of zirconium carrier were added to the initial target solution. Addition of barium ions caused the precipitation of barium fluorozirconate which was washed with water and dissolved in concentrated nitric acid containing 5% boric acid. The barium ion was eliminated by the addition of sulfuric acid. Zirconium hydroxide was formed by addition of ammonium hydroxide, and, after a water wash, it was dissolved in concentrated hydrochloric acid. The solution was adjusted to 6*N* hydrochloric acid and contacted with a 0.4*M* solution of thenolytrifluoroacetone (TTA) in benzene. The organic phase (containing the zirconium) was washed three times with 1*M* nitric acid and contacted with 4*N* hydrofluoric acid to back-extract the zirconium. The first part of the procedure was repeated up to the TTA extraction step. An aliquot of the solution was then precipitated by digestion with 16% mandelic acid. The zirconium tetramandelate was washed with hot water and filtered through a tared glass filter and again washed with water, alcohol, and ether. After drying for 10 min at 110°C, the sample was weighed and mounted. The chemical separation took about 1.5 h.

Copper Separation Procedure. Fifty milligrams of copper carrier and milligram quantities of salts of a number of elements near copper and niobium in atomic number were added to the dissolved target. Excess fluoride ions were removed by the standard method. Upon addition of an excess of ammonium hydroxide, the copper remained in solution as the ammonium complex while the niobium, and many other elements, precipitated as the hydroxide. The solution was adjusted to 2*N* hydrochloric acid and cupric sulfide was precipitated. Concentrated hydrochloric and nitric acids dissolved the sulfide, and the addition of sodium sulfite reduced the copper to the plus-one state. Addition of potassium thiocyanate precipitated cuprous thiocyanate which was dissolved with concentrated hydrochloric and nitric acids. Niobium, zirconium, yttrium, and iron ions were added and precipitated as mixed hydroxides to remove contaminants. The copper was then reduced to the metallic form by sodium hydrosulfite in a strongly basic solution. The metallic copper was dissolved in nitric acid, and the procedure was repeated starting at the thiocyanate precipitation. The copper was filtered through a weighed glass filter, washed with water and acetone, weighed, and mounted. Approximately 45 min were required for the separation.

Nickel Separation Procedure. Ten mg of nickel carrier, together with milligram quantities of a number of elements in the region of niobium, were added to the target solution. Following the elimination of the fluoride ions, an excess of ammonium hydroxide was added to precipitate the niobium and a number of the other hydroxides, leaving nickel in solution in the form of the ammonium complex. A copper sulfide precipitation was followed by a precipitation of the mixed hydroxides of zirconium, yttrium, and iron. The nickel was then precipitated with 1% dimethylglyoxime and redissolved in hydrochloric acid. A second copper sulfide precipitation succeeded by a dimethylglyoxime precipitation yielded a sample free from contamination. The precipitate was filtered through a tared glass filter and washed with water. After drying for 10 min at 110°C, the sample was weighed and mounted. The procedure took about one h.

Sodium Separation Procedure. Twenty mg of sodium carrier were added to the dissolved target, and the fluoride ions were eliminated. Addition of ammonium hydroxide precipitated the niobium. Copper was added to the supernate to precipitate cupric sulfide as a scavenge. Iron hydroxide was then precipitated for the same purpose. The solution was evaporated to dryness and 6*M* ammonium acetate was added. Sodium was

[30] Our procedures are based on those published in the following reports: Collected Radiochemical Procedures, Los Alamos Scientific Laboratory Report, LA-1721, Los Alamos, New Mexico, December 1954, (unpublished); W. W. Meinke, University of California Radiation Laboratory Report UCRL-432, August 1949 (unpublished).

precipitated by stirring with a solution of uranyl acetate, magnesium acetate, and acetic acid, and washed with a solution of glacial acetic acid, anhydrous ethyl acetate, and anhydrous ethanol. The sodium uranyl acetate was suspended in *n*-butanol. *n*-butanol saturated with dry hydrogen chloride was added to change the precipitate to sodium chloride which was washed with a solution of *n*-butanol and *n*-butanol saturated with hydrogen chloride. The sodium precipitation was repeated, and the organic material was expelled by heating. A small amount of potassium ion was added together with perchloric acid, and the solution fumed to dryness. *n*-butanol was added and the mixture was boiled to dissolve the sodium perchlorate. Sodium chloride was again precipitated from the supernate by addition of *n*-butanol saturated with hydrogen chloride. The precipitate was filtered through a tared glass filter, washed with *n*-butanol, dried for 10 min at 110°C, weighed, and mounted. The separation took approximately 3.5 h.

APPENDIX B. DETAILS OF ACTIVITY MEASUREMENTS

Niobium. The amounts of Nb^{89} and Nb^{90} in the purified niobium fraction were measured by the resolution of the decay curves taken in the proportional counter. Activity contributions from Nb^{91m}, Nb^{92}, and Nb^{95} were also observed but no quantitative measurement of them was attempted. For Nb^{89}, the experimentally observed half-life of 1.79 h was used in the analysis of the decay curve. The contribution to the Nb^{89} yield from decay of isobars of higher atomic number was estimated to be less than 10%. The growth of 79-h Zr^{89} into the sample interfered with the measurement of Nb^{90}; this interference was eliminated by repeating the niobium chemical separation 24 h after bombardment on an aliquot of the niobium fraction, after which the Nb^{90} could be observed free of Zr^{89} contamination. The measured Nb^{90} yield was judged to be the independent yield of this nuclide because of the expected low yield of Mo^{90} and because the 5.7-h Mo^{90} half-life is long compared to the time of the initial Nb separation.

Discovery of Niobium-88. During the course of these experiments, a 15-min positron activity was observed in the niobium fraction and it was established that this activity was the parent of Zr^{88}. This conclusion was confirmed by preparation of the Nb^{88} activity by the reaction of carbon nuclei with a bromine target in the Berkeley heavy ion linear accelerator.

Zirconium. Zr^{87}, Zr^{88}, and Zr^{89} were measured by analysis of the decay curves of the zirconium fractions taken on the proportional counter. Zr^{86} activity was also observed but certain difficulties in the measurement of this electron-capture activity prevented an absolute determination of yield. The proportional counter activity of the 85-d Zr^{88} was due to the conversion electrons of the 394-keV gamma transition present in 100% abundance. Quantitative measurements of the 394-keV photopeak in the NaI crystal counter made it possible to calibrate the beta counter for Zr^{88} counting. Measurement of the 79-h Zr^{89} was hampered by the growth of 80-h Y^{87} from the decay of its 1.6-h parent, Zr^{87}. This interference was eliminated by a second purification of an aliquot of zirconium 24 h after bombardment, when the Zr^{87} had decreased below detectability.

The complex decay curves were analyzed with a least squares program on an IBM 704 computer. Good fits were obtained for the three measured isotopes with half life values in agreement with published values.

The yield values for Zr^{87} and Zr^{88} include contributions from isobars of higher Z which were judged to be less than 20% of the total. The yield value of Zr^{89} contains only a slight contribution from Nb^{89} because less than 10% of the 1.79-h Nb^{89} could have decayed into Zr^{89} before the initial chemical separation was made.

In a few cases the results from the analysis of the proportional counter decay curves were checked by measurement of gamma ray photopeaks in the NaI crystal spectrometer and by application of known information on gamma ray energies and intensities.

Copper. Ten-min Cu^{62} and 5-min Cu^{66} were observed in copper fractions isolated by a rapid chemical procedure, but owing to experimental difficulties we did not complete an accurate determination of their yield. There was little difficulty in resolving 3.3-h Cu^{61}, 12.0-h Cu^{64}, and 62-h Cu^{67} components from the decay curve taken with the aid of the proportional counter on the copper fraction purified by the longer procedure described in Appendix A. The contributions of isobars of higher atomic number to the Cu^{67} yield is believed to be $<1\%$, and to the Cu^{61} yield, less than 10%.

Nickel. Ni^{57}, Ni^{65}, and Ni^{66} components were resolved from the decay curves taken in the proportional counter. Application of the Biller-plot method[31] helped in the separation of the 36-h Ni^{57} and 54.8-h Ni^{66}. The contribution of Cu^{57} to the Ni^{57} yield and of Co^{65} and Co^{66} to the yield of Ni^{65} and Ni^{66} is believed to be small as judged from the general observation of a rapid dropoff in yield with distance from the line of beta stability.

Sodium. A 15-h Na^{24} component and a constant Na^{22} component were resolved from the curves taken with the proportional counter. Calibration errors are small since the same nuclides were counted in the monitor foils. However, the counting rates for the 2.6-year Na^{22} were only 1 to 30 counts per min so that at times there was a considerable error in the subtraction of the background. The measured cross section values include contributions from isobars with $Z \neq 11$. Whether this contribution is large or small is difficult to estimate, since there is no systematic information on isobaric yields, and furthermore, the mode of production of these light products is unknown.

[31] W. F. Biller, University of California, Lawrence Radiation Laboratory, Report UCRL-2067, December 1952 (unpublished).